Identification of Variable Frequency Induction Motor Models From Operating Data

Amuliu Bogdan Proca, *Student Member, IEEE,* and Ali Keyhani, *Fellow, IEEE*

***Abstract*—The parameters of the induction motor model vary as operating conditions change. Accurate knowledge of these parameters and their dependency on operating conditions is critical for optimal field oriented control. This paper presents a systematic approach to modeling an induction motor considering operating conditions. All parameters are assumed to vary as a function of the operating conditions. The parameters are estimated from transient data using a constrained optimization algorithm. The parameters are mapped to the operating conditions using polynomial functions and artificial neural networks. The model is validated for both steady state and transient conditions.**

***Index Terms*—Induction motor model, operating conditions, parameter estimation, variable frequency.**

NOMENCLATURE

V_s	Stator voltage (rms value).
V_d, V_q	Voltages in stationary reference frame.
I_d, I_q	Stator currents in stationary reference frame.
I_d^e, I_q^e	Stator currents in synchronous reference frame.
λ_d, λ_q	Rotor fluxes stationary reference frame.
I_1, I_2	Stator and rotor currents (rms value).
φ	Phase shift between voltage and current.
$V=\sqrt{V_d^2+V_q^2}$	Stator voltage (peak value).
$I=\sqrt{I_d^2+I_q^2}$	Stator current (peak value).
ω_e, ω_r	Synchronous and mechanical frequency.
$s=\omega_s/\omega_e$	Slip.
ω_s	Slip frequency (rotor current frequency).
L_l, L_m	Magnetizing and leakage inductance.
R_s, R_r, R_c	Stator, rotor, and core loss resistance.
T_e	Produced electromagnetic torque.
n_p	Number of poles pairs.
$R_{r,c}$	Core loss resistance in parallel with R_r/s.
T	Rotor temperature.

I. INTRODUCTION

INDUCTION motors are used in automotive applications, either as stand-alone propulsion systems (electric vehicles) or in combination with an internal combustion engine (hybrid electric vehicles). Accurate knowledge of the induction motor model and its parameters is critical when field orientation techniques are used. The induction motor parameters vary with the operating conditions, as is the case with all electric motors. The inductances tend to saturate at high flux levels and the resistances tend to increase as an effect of heating and skin effect. Temperature can have a large span of values, load can vary anywhere from no-load to full load and flux levels can change as commanded by an efficiency optimization algorithm. It could then be expected that the model parameters also vary considerably.

Depending on the type of tests performed on the motor, the testing methods could be classified as the following.

Off Site Methods: Test the motor separately from its application site [3]–[9]. The motor is tested individually, in the sense that it is not necessarily connected to the load it is going to drive or in the industrial setup it is going to operate in. The most common such tests are the no-load test and the locked-rotor test. The advantage of the above methods is their simplicity. However, these tests usually represent poorly the real operating conditions of the machines (for example, they lack the effect of PWM switching on the machine parameters).

On Site and Off Line Methods: These tests are performed with the motor already connected in the industrial setup and supplied by its power converter [2], [10]–[14]. These tests are usually meant to allow the tuning of the controller parameters to the unknown motor it supplies and are also known as self-commissioning. As they are convenient for the controller manufacturer (one control program could work for different motors), they usually are less precise than the individual tests.

On-line methods, in which some parameters are estimated while the motor is running on-site [15]–[19], [22]. These methods are concerned usually with rotor parameters (L_m and R_r or the time constant, T_r) and assume that the other parameters are known. These methods usually perform well only for a good initial value of the parameter to be determined and for relatively small variations (within 10%).

The purpose of this paper is the development of an induction motor model with parameters that modify as a function of operating conditions. The development is on-site and off-line. While stator resistance is measured through simple dc test, the leakage inductance, the magnetizing inductance and the rotor resistance are estimated from transient data using a constrained optimization algorithm. Through a sensitivity analysis study, for each operating condition, the parameters to which the output error is less sensitive are eliminated. The parameters are estimated under all operating conditions and mapped to them (e.g., analytical functions relating parameters to operating conditions are created). A correlation analysis is used to isolate the operating conditions that have most influence on each parameter. A

Manuscript received November 29, 2000.

The authors are with the Electrical Engineering Department, The Ohio State University, Columbus, OH 43210 USA (e-mail: keyhani.1@osu.edu).

Publisher Item Identifier S 0885-8969(02)01512-7.

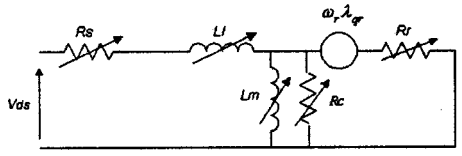

Fig. 1. Induction motor model in stationary reference frame (d-axis).

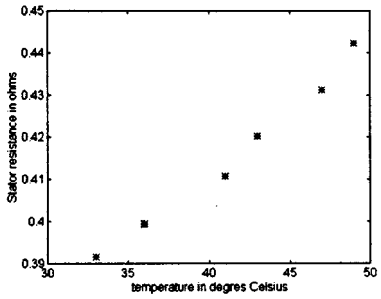

Fig. 2. Stator resistance as a function of temperature.

core loss resistance models core losses. This resistance is estimated using a power approach and artificial neural networks. No additional hardware is necessary. The authors used the same power converter and DSP board that controls the motor in the industrial setting to generate the signals necessary to model the motor. Therefore, phenomenons related to operation (for example PWM effects) are captured in modeling.

II. Induction Motor Model

Fig. 1 represents the induction motor model used in this research (d-axis, q-axis are similar). As noted by [1], the model is identical (without any loss of information) to the more common T-model in which the leakage inductance is separated in stator and rotor leakage. The core loss branch is added to account for both stator and rotor core losses.

III. Parameter Estimation

A. Estimation of R_s

The estimation of the stator resistance is based on a dc test. A small positive reference (that maintains the current below its rated value) is set between phases A–B and C–B using the power converter. R_s is calculated as

$$R_s = \frac{2}{3}\frac{V_{AB}}{I_B}. \tag{1}$$

To capture the effect of temperature on the stator resistance, before each test, the motor was run with a higher load. The stator resistance test was performed immediately after the motor stopped. The temperature of the stator winding was also measured. The temperature dependency of the stator resistance is shown in Fig. 2.

B. Estimation of L_m, L_l, and R_r

For this part of the estimation, the core loss resistance was neglected. However, since the core loss resistance is about 100–2000 times higher than the rotor resistance, the error introduced in the estimation of R_r, L_m, and L_l is minimal.

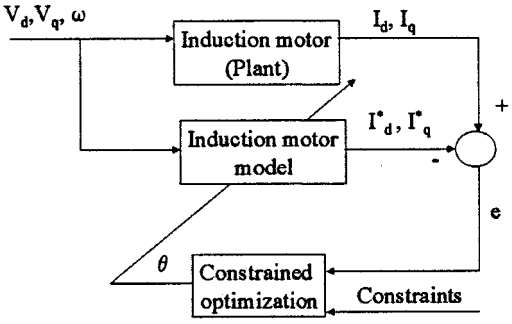

Fig. 3. Estimation block diagram.

Transient data was used to determine L_m, L_l, and R_r. The data consisted in small disturbance at steady state by stepping the supply voltage amplitude by 10%. The tests encompass a wide variation of frequency, supply voltage, and load. The frequency was varied from 30 Hz to 80 Hz in steps of 10 Hz. The supply voltage was varied from 10% to 100% of the rated voltage value in steps of 10% for each frequency. The load was varied from no-load to maximum load in eight steps. A total of 290 data files were obtained.

The estimation was performed using a constrained optimization method available in Matlab ("constr"). Fig. 3 shows the block diagram of the estimation procedure.

The induction motor model can be expressed in state space form as

$$\dot{X} = AX + BU \tag{2}$$

$$Y = C \cdot X \tag{3}$$

where

$$X = [I_q \quad I_d \quad \lambda_q \quad \lambda_d]^T$$

$$A = \begin{bmatrix} -\frac{R_s+R_r}{L_l} & 0 & \frac{R_r}{L_l L_m} & -\frac{\omega_r}{L_l} \\ 0 & -\frac{R_s+R_r}{L_l} & \frac{\omega_r}{L_l} & \frac{R_r}{L_l L_m} \\ -R_r & 0 & -\frac{R_r}{L_m} & \omega_r \\ 0 & R_r & -\omega_r & -\frac{R_r}{L_m} \end{bmatrix}$$

$$B = \frac{1}{L_l}\begin{bmatrix} 1 & 0 \\ 0 & 1 \\ 0 & 0 \\ 0 & 0 \end{bmatrix}$$

$$C = \begin{bmatrix} 1 & 0 & 0 & 0 \\ 0 & 1 & 0 & 0 \end{bmatrix} \text{ and } U = \begin{bmatrix} V_q \\ V_d \end{bmatrix}.$$

The initial conditions for the model were established as

$$X = [I_{q(0)} \quad I_{d(0)} \quad \hat{\lambda}_q \quad \hat{\lambda}_d]^T. \tag{4}$$

The error between model and measurements was calculated as

$$e = \sqrt{\sum_{k=1}^{N} \left(\hat{I}_{d(k)} - I_{d(k)}\right)^2 + \left(\hat{I}_{q(k)} - I_{q(k)}\right)^2}. \tag{5}$$

The constrained optimization function is used to minimize the error function by modifying the parameter vector θ

$$\theta = [L_m \quad R_r \quad L_l \quad \hat{\lambda}_{q(0)} \quad \hat{\lambda}_{d(0)}]. \tag{6}$$

The initial values of the fluxes are not normally included in the parameter vector since they can be calculated from the initial conditions of the currents at steady state. However, these currents are noise corrupted and their measurement error will propagate into the calculation of the initial values of the flux. Furthermore, since flux equations have a large time constant, the initial condition error would influence the flux observation over the entire transient measurement (the self-correction of an otherwise convergent flux observer [22] will not have the time to correct the initial condition error) and will yield erroneous parameter estimates.

The authors observed that the parameter vector modification increased the rate of convergence of the algorithm. Constraints on R_r, L_l, and L_m were imposed as 10% of the rated value for the lower bound and 300% for the upper bound. For $\lambda_{d(0)}$ and $\lambda_{d(0)}$ the constraints were imposed as $\pm 200\%$ of the saturation value (0.5 Wb).

IV. Sensitivity Analysis

Since an output error estimation method is used, there is no theoretical guarantee that the parameters will converge to their actual values. Therefore, it is necessary to study the effect of each parameter on the total error. It is obvious that those parameters with little effect on the total error will be more prone to estimation errors than parameters that affect it more.

At steady state, the squared error per period can be calculated as

$$e^2 = \frac{1}{T}\int_0^T E^2(t)dt = \frac{1}{2}\left(I^2 + \hat{I}^2 - 2\hat{I}\cdot I\cos(\varphi - \hat{\varphi})\right). \tag{7}$$

The sensitivity of the squared error to a parameter (y) can be expressed as

$$S_y^e = \frac{e^2\left(\hat{I}(y+\Delta y), I(y)\right)}{\Delta y}\cdot\frac{y}{I}. \tag{8}$$

For the proposed model, the steady state current (complex form) can be expressed as

$$\vec{I} = V\cdot\frac{\frac{R_r}{s} + jX_m}{-X_l X_m + \frac{R_s R_r}{s} + j\left(\frac{R_r}{s}(X_l + X_m) + R_s X_m\right)} \tag{9}$$

and I and φ are the module and phase angle of $\vec{I}$.

The sensitivity analysis was conducted for a slip ranging from 0 to 10% (larger values of s are unobtainable at steady state) and a frequency from 20 Hz to 100 Hz. The rated values of the parameters were used. Fig. 4 shows a comparison of sensitivity for R_r, L_m, and L_l at 60 Hz.

It can be seen that the sensitivity of the error to L_l or R_r is low at small slip. Large errors can be introduced at low slip since their effect on the error is small. A limit of 2% on the slip was imposed on the slip values. The L_l and R_r estimates below this value are discarded. For large values of the slip the sensitivity of the error to L_m decreases to 0. L_m estimates for slip values larger than 2% were discarded.

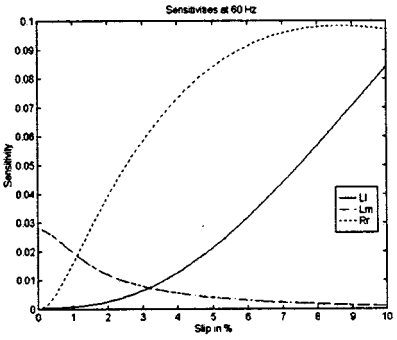

Fig. 4. Sensitivity of error to parameters as a function of slip at 60 Hz.

TABLE I
Correlation Between Parameters and Operating Conditions

Parameter	I_d^e	I_q^e	I	ω_s
L_m	-0.9287	0.0167	-0.6652	0.3473
R_r	0.1543	0.8061	0.8023	0.5485
L_l	-0.3212	-0.4264	-0.7135	0.0177

V. Parameter Mapping to Operating Conditions

Up to this point, the parameters of the motor were estimated for various operating conditions. The purpose of this section is to find the relation of the parameters to the operating conditions in a form that allows for use in a control environment. However, in order to be able to define an operating condition or to relate (map) a parameter to a condition, a correlation analysis is necessary. This establishes the "strong" and "weak" dependencies of parameters to operating variables. The authors selected intuitively the variables for the correlation study as I_d^e, I_q^e, I, and ω_s. It could be argued that temperature is also a factor in this mapping. However, since the only temperature measurement available was the stator temperature (and was used for stator resistance calculation) it was not used in this correlation study.

The correlation between two variables (in this case one variable is a parameter (y) and the other a operating condition variable (x)) can be defined as

$$C_{x,y} = \frac{\frac{1}{N-1}\sum_{k=1}^{N}((x_k - \bar{x})(y_k - \bar{y}))}{\sigma_x \sigma_y} \tag{10}$$

where $\bar{x}$, $\bar{y}$ are the mean of x and y, respectively, and σ_x, σ_y are their standard deviations. Table I shows the results of the correlation.

Mapping consists in expressing the parameters of the motor as analytical functions of the operating conditions.

A. Magnetizing Inductance, L_m

A strong correlation was observed between L_m and I_d^e. L_m clearly saturates with an increase in I_d^e. A second order polynomial was used to represent the dependency of L_m to I_d^e in the saturated region.

$$L_m(I_d^e) = k_1\cdot I_d^{e^2} + k_2\cdot I_d^e + k_3. \tag{11}$$

Fig. 5 shows a comparison between the polynominal and the results of the estimation.

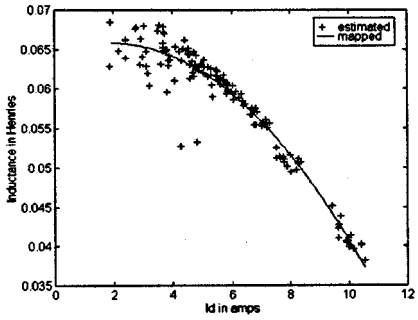

Fig. 5. L_m as function of I_d^e.

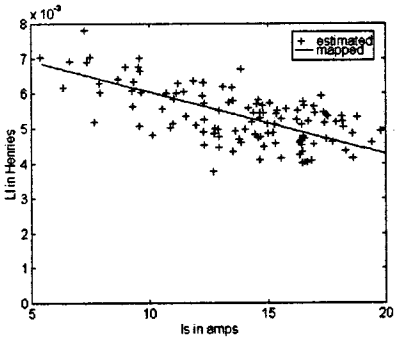

Fig. 6. L_l as function of I.

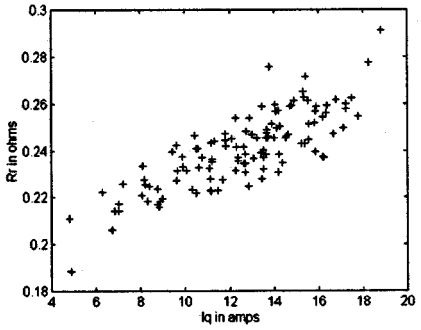

Fig. 7. R_r as function of I_q^e.

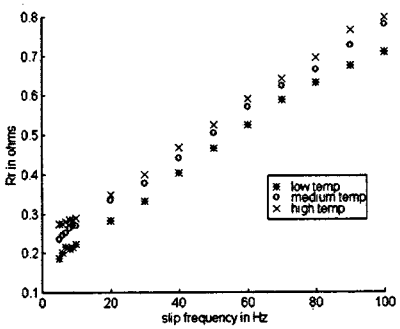

Fig. 8. Rotor resistance as function of ω_s for different temperatures.

B. Leakage Inductance, L_l

A strong correlation was also observed between L_l and I. L_l saturates with an increase in I. A linear approximation was used to represent the dependency of L_l to I.

$$L_l(I) = k_4 \cdot I + k_5. \tag{12}$$

Fig. 6 shows a comparison between the polynomial and the results of the estimation.

C. Rotor Resistance, R_r

Previous research has shown that the rotor resistance varies as a function of two factors: slip frequency (through skin effect) and rotor temperature (unmeasurable). However, Table I shows a correlation between R_r and ω_s but also I_q^e. The dependency is shown in Fig. 7. The correlation is due to the fact that both slip frequency and temperature are proportional to I_q^e. The authors observed that the $R_r(I_q^e)$ correlation holds only if the motor runs for a few minutes at a certain operating condition, to allow for temperature to reach a steady state.

A sudden variation in I_q^e would not determine a sudden change in R_r if slip frequency remains constant since temperature does not change as fast. Therefore, the $R_r(I_q^e)$ relation can only be used at steady state. In order to establish the influence of slip frequency on R_r, a test similar to a locked rotor was used. The difference consists was that the rotor was not mechanically locked, but the voltages were small enough that the rotor would not move. The frequency was varied between 5 Hz and 120 Hz (1 Hz increments in the 5–10 Hz region and 10 Hz increments for the rest). Prior to each series of tests, the motor was run under a loading condition (no-load, medium load, and full load) to assure heating of the rotor.

A temperature sensor was mounted on the stator. This sensor was used for an indication when temperature has reached a steady state (for each loading condition). Fig. 8 shows the results of the R_r estimation as a function of slip frequency (for locked rotor, equal to stator frequency).

Since rotor temperature measurements are hardly possible, a precise off-line mapping of rotor resistance to operating conditions is impossible. However, the linearity relation (within the range of interest) between rotor resistance and slip frequency can be used for R_r calculation. An on-line observer was developed (see Appendix). The observer is based on the assumptions that the rotor temperature varies much slower than the other variables (current, speed, etc.) and that steady state operating conditions exist (e.g., the motor is not in continuous transient). The rotor resistance dependency to slip frequency and rotor temperature can be expressed as

$$R_r(\omega_s, T) = R_1(T) + k_6 \cdot \omega_s \tag{13}$$

in which $R_1(T)$ is the influence of temperature (unknown).

The coefficient k_6 (influence of slip frequency) was estimated off line from the locked rotor tests measurements. At each operating condition (steady state), the values of the rotor resistance and of the slip frequency are estimated with the observer. Then for each loading condition (temperature)

$$\hat{R}_1(T) = \hat{R}_r(\omega_s, T) - k_6 \cdot \hat{\omega}_s. \tag{14}$$

Assuming that temperature changes slowly, at each instant of time, knowing the slip frequency allows for the determination of rotor resistance. Each time a steady state condition is detected, $R_1(T)$ is reevaluated and rotor resistance calculated as function of slip frequency. It can be argued that since rotor resistance is

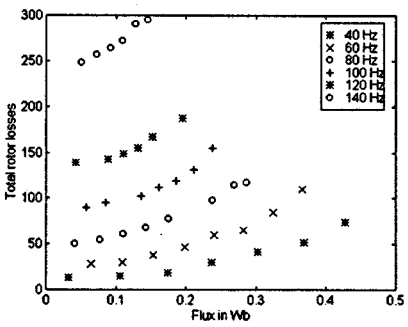

Fig. 9. Rotor power losses for no-load test.

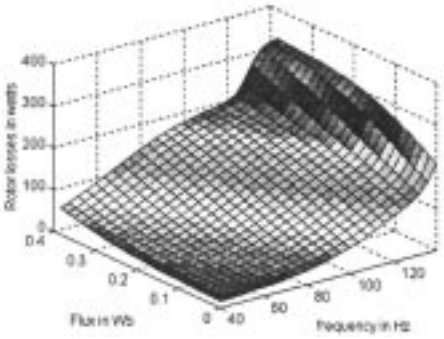

Fig. 10. Mapping of rotor losses using ANN.

estimated, there is no need in determining $R_1(T)$. This is true while the motor operates at steady state. However, for efficiency optimization it is important to predict the variation of rotor resistance prior to a new steady state condition.

VI. Core Loss Estimation

The disparity in values of rotor resistance and core loss resistance makes the simultaneous estimation of both close to impossible using a constrained optimization method. That is because the core loss resistance has a much smaller effect on the model output than the rotor resistance (i.e., a smaller sensitivity). One should also note that since the slip is nonzero for the no-load test and R_r is already known, R_c could be theoretically calculated from $R_{r,c}$ at steady-state. However, even for most precise speed encoders, the error in calculating a slip approaching zero could translate in an order of magnitude of error when calculating R_r/s.

The authors used a power-based approach for calculating the core resistance. The procedure is shown in the following.

A. Calculate Rotor Losses at Frequencies of Interest

Use the no-load tests and calculate the rotor power losses for each data set

$$P_{\text{rotor}} = V_s I_1 \cos(\varphi) - R_s I_1^2. \tag{15}$$

A plot of these losses is shown in Fig. 9 for various frequencies. The losses increase with both the frequency and the rotor flux.

B. Calculate Friction and Windage Losses

Since core losses are zero when flux is zero, the intersection of the power curves with the vertical axis determines the friction and windage losses for a specific frequency. To find the friction and windage losses for all frequencies, an ANN was used to map the rotor losses to frequency and flux. More details on using ANN for mapping can be found in [3]. The mathematical relationship between the input and output patterns can be described as

$$P_{\text{rotor\_losses}} = N_d(\lambda, \omega_e) \tag{16}$$

where N_d is a nonlinear neural network mapping to be established. The ANN used in this study consists of two processing elements in the input layer. A single processing element in the output layer corresponds to the losses being modeled. The number of elements in the hidden layer is arbitrarily chosen depending on the complexity of the mapping to be learned. A hyperbolic tangent $(\tanh)$ transfer function is used in all hidden layer elements, while all elements in the input layer and output layer have linear (1:1) transformations. The back-propagation algorithm is used to train the neural network such that the sum squared error E between actual network outputs O and corresponding desired outputs ζ is minimized over all training patterns μ.

After estimating the nonlinear mapping N_d of (16) in terms of the neural network, the network output $P_{\text{rotor\_losses}}$ is computed from the 2×1 input vector P according to the following equation:

$$P_{\text{rotor\_losses}} = W_2 \cdot \tanh(W_1 \cdot P + B_1) + B_2. \tag{17}$$

W_2 denotes the matrix of connecting weights from the hidden layer to the output layer. W_1 is the weight matrix from the input-layer to the hidden-layer. Bias terms B_2 and B_1 are used as connection weights from an input with a constant value of one. The training patterns for the neural network models are composed of the no-load test data. Each data set is a vector of λ, ω_e, and $P_{\text{rotor\_losses}}$. The results of the mapping are shown in Fig. 10. Friction and windage losses can be calculated for ANN at zero flux. A deterministic approach could have been used for determining windage and friction losses. However, such an approach would have required the use of a dynamometer to isolate windage and friction losses (they are a part of the total rotor losses). Furthermore, since an ANN model for total rotor losses was already developed, calculating windage and friction losses was seamless.

C. Calculate Core Losses

Core losses for each frequency and flux can be determined by subtracting the friction and windage losses and from the rotor losses (resistive rotor losses can be neglected at small slip).

$$P_{\text{core}}(\omega, \lambda_{dr}) = P_{\text{rotor\_losses}}(\omega, \lambda_{dr}) - P_{f\&w}(\omega_r) \tag{18}$$

$$\text{where } P_{f\&w} = P_{\text{rotor\_losses}}(\omega, 0) = N_d(\omega, 0). \tag{19}$$

D. Calculate Core Resistance

For each data point, calculate the core loss resistance (see Fig. 1) as

$$R_c(\omega_e, \lambda_{dr}) = \frac{P^2_{\text{rotor\_losses}}(\omega_e, \lambda_{dr})}{I_2^2 \cdot P_{\text{core}}(\omega_e, \lambda_{dr})}. \tag{20}$$

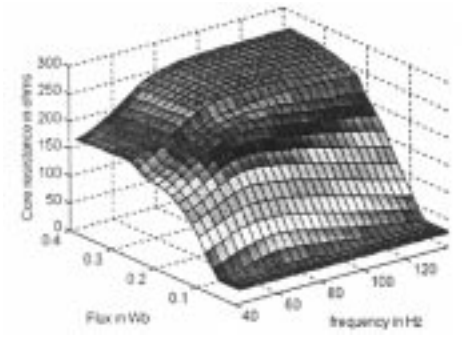

Fig. 11. Rotor core loss as function of flux and frequency.

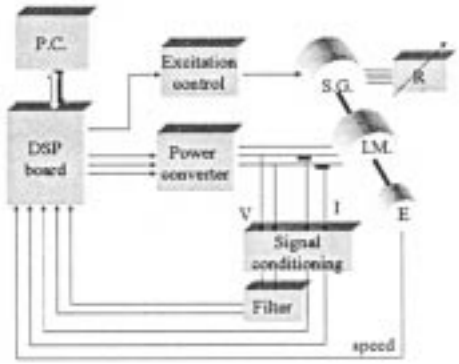

Fig. 12. Experimental setup.

TABLE II
INDUCTION MOTOR PARAMETERS (RATED)

R_s	0.39 Ω
L_l	0.006 Henry
L_m	0.068 Henry
R_r	0.22 Ω

Map the core loss resistance to flux and frequency using ANN. The procedure is similar to the rotor loss mapping. Fig. 11 presents the results of the mapping.

VII. EXPERIMENTAL SETUP

The experimental setup used in this research is shown in Fig. 12. The induction motor is 3 phase, 4 pole, 5 Hp, 1750 rpm 220 V squirrel cage. The rated parameters of the motor are shown in Table II.

The load is a 5 Hp synchronous generator supplying a variable resistor box. A variable dc power supply controls the excitation of the synchronous generator. The power converter is rated at 400 V/30 A and can switch at 20 kHz. A dual processor (TMS320C31 Master and TMS320P14 Slave) DSP board is used both for control and data acquisition. In order to avoid aliasing, the measured voltage is passed through a low pass filter prior to being acquired. The synchronous generator can be controlled simultaneously with the motor using the DSP board. The control is realized through the excitation voltage. The PWM cycle is 240 μs and the data acquisition sampling time is 60 μs. These values were chosen to accommodate the control algorithm and analytical model computation. Except for the ANN part, the analytical model is not very computational intense. The ANN part could not be implemented online with the TMS320C31 (it would have required a considerable increase in the control loop that would make the overall control scheme worse than without it). The authors expect that with the continuous increase in processing power of DSPs this will not be a problem in the future.

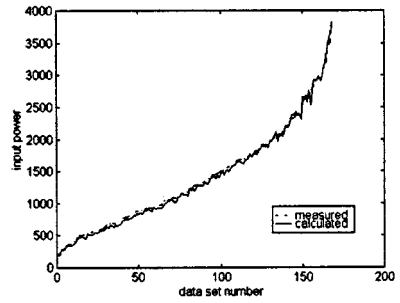

Fig. 13. Measured and calculated input power.

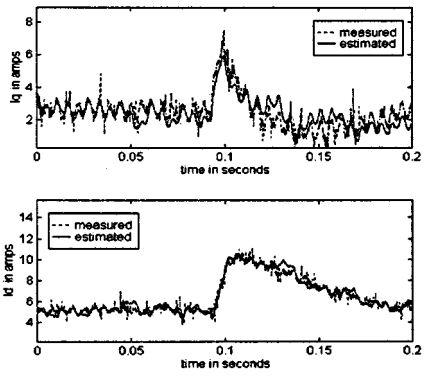

Fig. 14. Estimation validation for 30 Hz test.

VIII. MODEL VALIDATION

A. Steady State-Power Input

In order to validate the model at steady state, the authors used tests encompassing the entire range of operation of the induction motor. The frequency of the motor was varied from 30 to 70 Hz. The supply voltage was varied from 10% to 100% of rated. For each voltage and frequency entry, the load was varied from zero to maximum value. For all data sets, input power was measured and compared to the input power calculated using measured voltage and speed and the model. Fig. 13 shows the results of the comparison.

B. Dynamic

The model was used to predict the transient performance. Each test consisted in a large voltage step (20%) applied while the motor was running at steady state. Tests were conducted at various frequencies and voltages and loads. Figs. 14–16 present examples of the results in terms of the synchronously rotating reference frame currents. A second type of test consisted in transient behavior when starting the motor. The start-up currents (measured and simulated) are shown in the Fig. 17 in synchronous reference frame. For comparison, the simulation where constant parameters (rated values) are used is shown in Fig. 18.

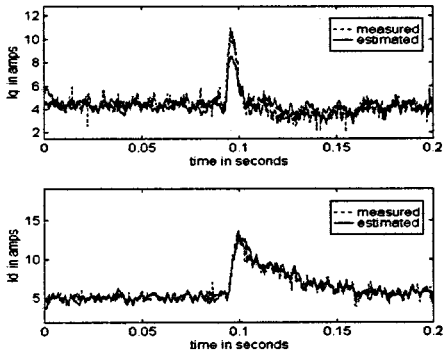

Fig. 15. Estimation validation for 60 Hz test.

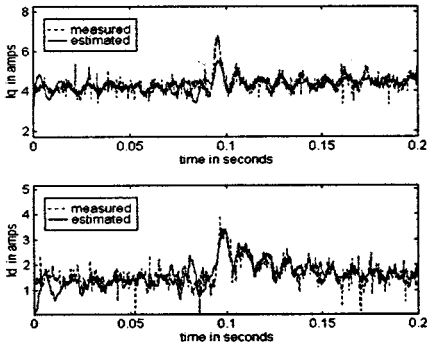

Fig. 16. Estimation validation for 90 Hz test.

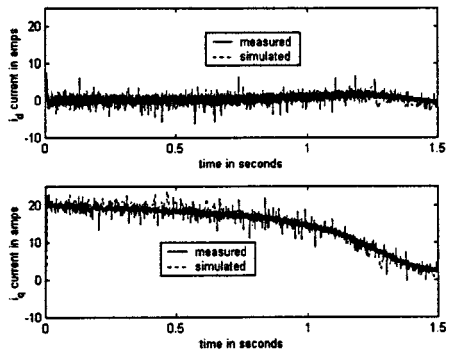

Fig. 17. Transient response for start-up from zero speed.

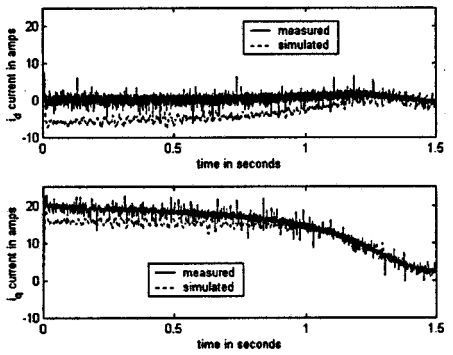

Fig. 18. Transient response for start-up from zero speed with rated fixed parameters.

IX. Conclusion

A systematic procedure for induction motor modeling was developed in this paper. The model includes the effects of inductance saturation (both for magnetizing and leakage inductance) and the effects of the core losses. It is also shown that there is a variation of rotor resistance as a function of slip frequency. The leakage inductance, magnetizing inductance and rotor resistance are estimated from transient data information using a constrained optimization method.

Sensitivity analysis is employed to show that error sensitivity to parameters varies as a function of slip. The analysis eliminates parameters with that yield low sensitivity. Analytical functions are used to map the parameters to operating conditions. Since rotor resistance depends on temperature and slip frequency and the former is not measurable, an on-line rotor resistance observer was developed. Core losses are estimated using a power approach. ANN are used to map the total rotor losses (iron losses, friction, and windage losses) to flux and frequency. The core losses are obtained by subtracting the rotor losses at zero flux (generated by the ANN) from the rotor loss surface. The model is validated using tests covering various operating conditions. Since efficiency optimization is sought with this model, the model is shown to correctly predict the power input of the motor. For dynamic validation, input voltage disturbance tests and start-from-zero tests were employed. The model correctly predicted both tests.

Appendix
Rotor Resistance Observer

The motor is operating at steady state.

a) Determine the supply frequency from current zero crossing.

b) Calculate slip frequency and slip as: $\omega_s = \hat{\omega}_e - \omega_r n_p$, $s = \omega_s/\hat{\omega}_e$ continue if slip is larger than 2%.

c) Filter currents with digital filter similar to the hardware based filter for voltages (see Section VIII) to account for the delay in voltage signals.

d) Transform the variables into d–q stationary reference frame and calculate the instantaneous values of V and I

$$V = \sqrt{V_q^2 + V_d^2}, \quad I = \sqrt{I_q^2 + I_d^2}.$$

e) Calculate $\sin(\omega t)$ and $\cos(\omega t)$ assuming $i_{\rm ds}$ and $i_{\rm qs}$ are reference phasors: $\sin(\omega t) = I_d/I$, $\cos(\omega t) = I_q/I$.

f) The voltage expression (d-axis) can be written as

$$\begin{aligned} y_n =& \frac{V_d(t)}{V} = \sin(\omega t + \varphi) \\ =& \sin(\omega t)\cos(\varphi) + \cos(\omega t)\sin(\varphi) = h_n \cdot \theta_n \end{aligned}$$

where $h_n = [\sin(\omega t)\ \cos(\omega t)]$, $\theta_n = [\sin(\varphi)\ \cos(\varphi)]$.
Initialize $P_1^{-1} = h_1' \cdot h_1$.

g) Recursively estimate θ_{n+1} using least squares

$$\begin{aligned} P_n^{-1} =& P_n^{-1} + h_n' \cdot h_n, \quad k_{w,n} = P_n \cdot h_n' \\ \theta_{n+1} =& \theta_n + k_{w,n} \cdot (y_n - h_n \cdot \theta_n). \end{aligned}$$

Calculate $\varphi = a\cos\left(\theta_N(1)/\sqrt{\theta_N(1)^2 + \theta_N(2)^2}\right)$.

Calculate rotor resistance

$$R_r = s\left(\frac{V}{I}\cos(\varphi) - R_s + \frac{\left(\omega L_m - \sqrt{(\omega L_m)^2 - 4\left(\frac{V}{I}\cos(\varphi) - R_s\right)^2}\right)^2}{4\left(\frac{V}{I}\cos(\varphi) - R_s\right)}\right).$$

REFERENCES

[1] G. R. Slemon, "Modeling of induction machines for electric drives," *IEEE Trans. Ind. Applicat.*, vol. 25, pp. 1126–1131, Nov./Dec. 1989.

[2] N. R. Klaes, "Parameter identification of an induction machine with regard to dependencies on saturation," *IEEE Trans. Ind. Applicat.*, vol. 29, pp. 1135–1140, Nov./Dec. 1993.

[3] S. I. Moon, A. Keyhani, and S. Pillutla, "Nonlinear neural-network modeling of an induction machine," *IEEE Trans. Contr. Syst. Technol.*, vol. 7, pp. 203–211, Mar. 1999.

[4] J. A. de Kock, F. S. van der Merwe, and H. J. Vermeulen, "Induction motor parameter estimation through an output error technique," *IEEE Trans. Energy Conv.*, vol. 9, pp. 69–76, Mar. 1994.

[5] A. M. N. Lima, C. B. Jacobina, and E. B. F. de Souza, "Nonlinear parameter estimation of steady-state induction machine models," *IEEE Trans. Ind. Electron.*, vol. 44, pp. 390–397, June 1997.

[6] L. A. de Souza Ribeiro, C. B. Jacobina, and A. M. N. Lima, "Linear parameter estimation for induction machines considering the operating conditions," *IEEE Trans. Power Electron.*, vol. 14, pp. 62–73, Jan. 1999.

[7] P. Pillay, R. Nolan, and T. Haque, "Application of genetic algorithms to motor parameter determination for transient torque calculations," *IEEE Trans. Ind. Applicat.*, vol. 33, pp. 1273–1282, Sept. 1997.

[8] E. Mendes and A. Razek, "A simple model for core losses and magnetic saturation in induction machines adapted for direct stator flux orientation control," in *Proc. Fifth Int. Conf. Power Electron. Variable-Speed Drives*, vol. 388, London, U.K., 1994, pp. 192–197.

[9] S. Ansuj, F. Shokooh, and R. Schinzinger, "Parameter estimation for induction machines based on sensitivity analysis," *IEEE Trans. Ind. Applicat.*, vol. 25, pp. 1035–1040, Nov./Dec. 1989.

[10] J. Stephan, M. Bodson, and J. Chiasson, "Real-time estimation of the parameters and fluxes of induction motors," *IEEE Trans. Ind. Applicat.*, vol. 30, pp. 746–759, May/June 1994.

[11] X. Xu and D. W. Novotny, "Implementation of direct stator flux orientation control on a versatile DSP based system," *IEEE Trans. Ind. Applicat.*, vol. 27, pp. 694–700, July/Aug. 1991.

[12] J. K. Seok, S. I. Moon, and S. K. Sul, "Induction machine parameter identification using PWM inverter at standstill," *IEEE Trans. Energy Conv.*, vol. 12, pp. 127–132, June 1997.

[13] C. Wang, D. W. Novotny, and T. A. Lipo, "An automated rotor time constant measurement system for indirect field-oriented drives," *IEEE Trans. Ind. Applicat.*, vol. 24, pp. 151–159, Jan./Feb. 1988.

[14] Y. N. Lin and C. L. Chen, "Automatic IM parameter measurement under sensorless field-oriented control," *IEEE Trans. Ind. Electron.*, vol. 46, pp. 111–118, Jan./Feb. 1999.

[15] S. K. Sul, "A novel technique of rotor resistance estimation considering variation of mutual inductance," *IEEE Trans. Ind. Applicat.*, vol. 25, pp. 578–587, July/Aug. 1989.

[16] T. Noguchi, S. Kondo, and I. Takahashi, "Field-oriented control of an induction motor with robust on-line tuning of its parameters," *IEEE Trans. Ind. Applicat.*, vol. 33, pp. 35–42, Jan./Feb. 1997.

[17] L. C. Zai, C. L. DeMarco, and T. A. Lipo, "An extended Kalman filter approach to rotor time constant measurement in PWM induction motor drives," *IEEE Trans. Ind. Applicat.*, vol. 28, pp. 96–104, Jan./Feb. 1992.

[18] D. J. Atkinson, P. P. Acarnley, and J. W. Finch, "Observers for induction motor state and parameter estimation," *IEEE Trans. Ind. Applicat.*, vol. 27, pp. 1119–1127, Nov./Dec. 1991.

[19] S. Wade, M. W. Dunnigan, and B. W. Williams, "New method of rotor resistance estimation for vector-controlled induction machines," *IEEE Trans. Ind. Electron.*, vol. 44, pp. 247–257, Apr. 1997.

[20] K. Matsuse, T. Yoshizumi, S. Katsuta, and S. Taniguchi, "High response flux control of direct-field-oriented induction motor with high efficiency taking core loss into account," *IEEE Trans. Ind. Applicat.*, vol. 35, pp. 62–69, Jan./Feb. 1999.

[21] B. Robyns, P. A. Sente, H. A. Buyse, and F. Labrique, "Influence of digital current control strategy on the sensitivity to electrical parameter uncertainties of induction motor indirect field-oriented control," *IEEE Trans. Power Electron.*, vol. 14, pp. 690–699, July 1999.

[22] K. Akatsu and A. Kawamura, "Online rotor resistance estimation using the transient state under the speed sensorless control of induction motor," *IEEE Trans. Power Electron.*, vol. 15, pp. 553–560, May 2000.

[23] S. J. Chapman, *Electric Machinery Fundamentals*, 2nd ed. New York: McGraw-Hill, 1991.

Amuliu Bogdan Proca (S'96) received the B.S. degree from Universitatea Politehnica Bucharest, Bucharest, Romania, and the M.S.E.E. and Ph.D. degrees from The Ohio State University (OSU), Columbus, in 1992, 1997, and 2001, respectively. His research interests are in the areas of permanent magnet synchronous machine modeling, parameter estimation, and design.

Ali Keyhani (S'72–M'76–SM'89–F'98) received the Ph.D. degree from Purdue University, West Lafayette, IN, in 1975.

From 1967 to 1969, he worked for Hewlett-Packard Co., Palo Alto, CA, on the computer aided design of electronic transformers. Currently, he is a Professor of Electrical Engineering at The Ohio State University, Columbus. From 1970 to 1973, he worked for Columbus and Southern Ohio Electric Company on computer applications for power system engineering problems. In 1974, he joined TRW Controls and worked on the development of computer programs for energy control centers. From 1976 to 1980, he was a Professor of Electrical Engineering at Tehran Polytechnic University, Tehran, Iran. His research interests are in control and modeling, parameter estimation, failure detection of electric machines, transformers, and drive systems.